Available online at www.sciencedirect.com
SCIENCE DIRECT®
Journal of Computational Physics 215 (2006) 552–565
JOURNAL OF COMPUTATIONAL PHYSICS
www.elsevier.com/locate/jcp

Exact nonreflecting boundary conditions for one-dimensional cubic nonlinear Schrödinger equations

Chunxiong Zheng

Department of Mathematical Sciences, Tsinghua University, Beijing 100084, PR China

Received 19 July 2005; received in revised form 18 October 2005; accepted 7 November 2005
Available online 20 December 2005

Abstract

The numerical approximation of one-dimensional cubic nonlinear Schrödinger equations on the whole real axis is studied in this paper. Based on the work of A. Boutet de Monvel, A.S. Fokas and D. Shepelsky [Lett. Math. Phys., 65(3): 199–212, 2003], a kind of exact nonreflecting boundary conditions are derived on the artificially introduced boundary points. The related numerical issues are discussed in detail. Several numerical tests are performed to demonstrate the behaviour of the proposed scheme.

Keywords: Nonlinear Schrödinger equation; Unbounded domains; Nonreflecting boundary conditions

1. Introduction

In this paper, we study the numerical approximation of 1-D cubic nonlinear Schrödinger (NLS) equations of the following form

$$\begin{aligned} &\mathrm{i}q_t + \partial_x^2 q - 2\rho|q|^2 q = 0 \quad x \in \mathbb{R}, \ \ t > 0, \\ &q(x,0) = q_0(x) \quad x \in \mathbb{R} \end{aligned} \tag{1}$$

where the real parameter ρ corresponds to a focusing ($\rho = -1$) or defocusing ($\rho = 1$) effect of the cubic nonlinearity. The NLS equation is connected to many applications in science and technology. For example, it has been tied to the motion of a vortex filament in inviscid incompressible fluids with the transformation of Hasimoto [13], and it has also been used to model the fiber architecture of aortic heart valve leaflets [16].

The unboundedness of the definition domain of problem (1) presents a great numerical challenge, since any standard domain-based method, such as finite element or finite difference, can only deal with a system of finite degrees of freedom, and this is impossible when the definition domain is unbounded. Thus, a basic numerical treatment of problem (1) is to restrict the computational domain to a finite interval $\Omega = (a, b)$ by introducing

E-mail address: czheng@math.tsinghua.edu.cn.

0021-9991/$ - see front matter
doi:10.1016/j.jcp.2005.11.005

two artificial boundary points $\Sigma = \{a, b\}$, and to consider a new Schrödinger problem defined only in Ω. To complete the new problem, two boundary conditions are necessary. The ideal ones, which will be given in this paper, should not only be easy to implement, but make the solution of the new problem be exactly the same as that of problem (1), namely, the waves originated from Ω are not (or at least not significantly) reflected when they travel to the boundary points of Σ. If this property holds for the new problem, the boundary conditions are usually said to be nonreflecting or transparent in the literature.

For the linear Schrödinger equations, how to derive the nonreflecting boundary conditions (NRBC) has been widely studied by many authors. The readers are referred to [4,2,6,12]. But for the nonlinear Schrödinger equations, the things turn to be much more complicated. A common treatment is to impose the homogeneous Dirichlet boundary conditions on the boundary points [5,7,19,20]. This is reasonable only if the computational interval is large enough, such that before the ending time point, the energy of the waves travelling to the boundary points are satisfactorily small. Obviously, this treatment is not economical from the computational point of view. An exception worth to be mentioned to solve this problem is the work by Antoine, Besse and Descombes [3]. They developed a constructive approach and derived some approximate nonlinear NRBCs based on the theory of pseudodifferential operators. The numerical tests given in their paper showed that their boundary conditions are quite efficient for simulating the propagation of fast enough solitons, while a loss of accuracy occurs for slower ones.

In this paper, as stated above, we will present a kind of exact NRBCs for the considered problem. Compared with the approximate boundary conditions, the exact NRBCs have an unlimited potential to present the numerical solutions with any prescribed accuracy. Our NRBCs are based on the work [10] of A. Boutet de Monvel et al., in which they derived a general relation between the Dirichlet and the Neumann data on the artificial boundary points. Unfortunately, this relation is unsuitable for the numerical purpose. We will derive some equivalent relations by doing some calculus and study its related discrete issues in detail.

The organization of this paper is as follows. In Section 2, we present the exact NRBCs which are suitable for the numerical treatment, and in Section 3, we deal with the numerical issues. We will propose a series of numerical schemes and discuss the related computational issues in detail. Some numerical tests are given in Section 4 to verify the accuracy and analyze the capacity of the proposed schemes. We conclude this paper in Section 5.

2. Exact nonreflecting boundary conditions

We assume that the initial function $q_0(x)$ is compactly supported in a finite interval $\Omega = (a, b) \subset \mathbb{R}$, with $b > a$. To seek the numerical solution of problem (1) in Ω, two NRBCs are needed to be imposed on the two boundary points $\Sigma = \{a,b\}$. In [10], a kind of exact NRBCs in the form of a generalized Dirichlet-to-Neumann (DtN) mapping were presented with the inverse scattering theory by analyzing the following problem

$$\begin{aligned} &\mathrm{i}q_t + q_{xx} - 2\rho|q|^2 q = 0 \quad x \in (-\infty, a) \cup (b, +\infty), \ \ t > 0, \\ &q(x, 0) = 0 \quad x \in (-\infty, a) \cup (b, +\infty). \end{aligned} \tag{2}$$

For example, let $g_0(t) = q(b,t)$ and $g_1(t) = q_n(b,t)$. According to Eq. (13) in [10], g_1 and g_0 are related by

$$g_1(t) = g_0(t)M_2(t,t) + \frac{4\mathrm{i}}{\pi}\int_{\partial D}\left[2k^2\int_0^t \mathrm{e}^{4\mathrm{i}k^2(\tau-t)}M_1(t, 2\tau - t)\,\mathrm{d}\tau - \frac{M_1(t,t)}{2i}\right]\mathrm{d}k, \tag{3}$$

where $\{M_j(t,s)\}_{j=1,2}$, together with $\{L_j(t,s)\}_{j=1,2}$, are determined by the following equations

$$L_1(t,t) = \frac{\mathrm{i}}{2}g_1(t), \ M_1(t,t) = g_0(t), \quad L_2(t,-t) = M_2(t,-t) = 0, \tag{4}$$

$$L_{1_t} - L_{1_s} = \mathrm{i}g_1(t)L_2 + \alpha(t)M_1 + \beta(t)M_2, \tag{5}$$

$$L_{2_t} + L_{2_s} = -\mathrm{i}\rho\bar{g}_1(t)L_1 - \alpha(t)M_2 + \rho\bar{\beta}(t)M_1, \tag{6}$$

$$M_{1_t} - M_{1_s} = 2g_0(t)L_2 + \mathrm{i}g_1(t)M_2, \tag{7}$$

$$M_{2_t} + M_{2_s} = 2\rho\bar{g}_0(t)L_1 - \mathrm{i}\rho\bar{g}_1(t)M_1, \tag{8}$$

$$\alpha(t) = \frac{\rho}{2}(g_0\bar{g}_1 - \bar{g}_0 g_1),\ \beta(t) = \frac{\mathrm{i}}{2}(\dot{g}_0 + i\rho|g_0|^2 g_0). \tag{9}$$

Here, D denotes the first quadrant of the complex k-plane, i.e.,

$$D = \{k \in C | \mathrm{Re}\, k > 0,\ \mathrm{Im}\, k > 0\},$$

and ∂D denotes its boundary. The contour integral in (3) is understood in the sense of primary value, and the orientation is from $+\mathrm{i}\infty$ to 0 on the imaginary axis, and then to $+\infty$ on the real axis. We should note that there is a misprint in the expression of function β in [10].

Theoretically, if the Dirichlet function $g_0(t)$ is prescribed, substituting Eq. (3) into Eqs. (4)–(9) gives a system of nonlinear PDEs for $\{L_j, M_j\}_{j=1,2}$ in terms of $g_0(t)$. After solving this system (the solvability is still an open problem), the Neumann function $g_1(t)$ can then be determined by Eq. (3). For convenience of reference, we explicitly formulate this mapping from $g_0(t)$ to $g_1(t)$ as

$$g_1(t) = \mathscr{K}(t; g_0). \tag{10}$$

Owing to the involvement of a double integral, Eq. (3) is unsuitable for the numerical treatment. Using the integral identity

$$\int_{\partial D} \frac{1 - \mathrm{e}^{-\mathrm{i}k^2}}{k^2}\,\mathrm{d}k = 2\sqrt{\pi}\mathrm{e}^{\mathrm{i}\pi/4}, \tag{11}$$

we can derive an equivalent equation. For any fixed $t > 0$, let $f(\tau) = M_1(t, 2\tau - t)$ and

$$I = \int_{\partial D}\left[2k^2\int_0^t \mathrm{e}^{4\mathrm{i}k^2(\tau - t)} f(\tau)\,\mathrm{d}\tau - \frac{M_1(t,t)}{2\mathrm{i}}\right]\mathrm{d}k.$$

From (7) and (4), we have $f(0) = M_1(t, -t) = 0$. Furthermore, Integrating by parts gives

$$\begin{aligned} I &= \int_{\partial D}\left[\frac{1}{2\mathrm{i}}\int_0^t f(\tau) d\mathrm{e}^{4\mathrm{i}k^2(\tau - t)} - \frac{M_1(t,t)}{2\mathrm{i}}\right]\mathrm{d}k = -\frac{1}{2\mathrm{i}}\int_{\partial D}\int_0^t f'(\tau)\mathrm{e}^{4\mathrm{i}k^2(\tau - t)}\,\mathrm{d}\tau\,\mathrm{d}k \\ &= -\frac{1}{2\mathrm{i}}\int_{\partial D}\int_0^t f'(\tau) d\frac{\mathrm{e}^{4\mathrm{i}k^2(\tau - t)} - 1}{4\mathrm{i}k^2}\,\mathrm{d}k = -\frac{1}{2\mathrm{i}}\int_{\partial D}\left[\frac{f'(0)(1 - \mathrm{e}^{-4\mathrm{i}k^2 t})}{4\mathrm{i}k^2} + \int_0^t \frac{1 - \mathrm{e}^{-4\mathrm{i}k^2(t-\tau)}}{4\mathrm{i}k^2} f''(\tau)\,\mathrm{d}\tau\right]\mathrm{d}k \\ &= -\frac{1}{2\mathrm{i}}\left[\frac{f'(0)}{4\mathrm{i}}\sqrt{4t} + \int_0^t \frac{\sqrt{4(t-\tau)}}{4\mathrm{i}} f''(\tau)\,\mathrm{d}\tau\right] 2\sqrt{\pi}\mathrm{e}^{\mathrm{i}\pi/4} = \frac{\sqrt{\pi}}{4}\mathrm{e}^{\mathrm{i}\pi/4}\int_0^t \frac{f'(\tau)}{\sqrt{t-\tau}}\,\mathrm{d}\tau. \end{aligned}$$

Substituting this equality into (3), we obtain

$$g_1(t) = g_0(t)M_2(t,t) - \frac{\mathrm{e}^{-\mathrm{i}\pi/4}}{\sqrt{\pi}}\int_0^t \frac{\partial_\tau M_1(t, 2\tau - t)}{\sqrt{t-\tau}}\,\mathrm{d}\tau = g_0(t)M_2(t,t) - \mathrm{e}^{-\mathrm{i}\pi/4}\partial_\tau^{1/2} M_1(t, 2\tau - t)|_{\tau = t}, \tag{12}$$

where $\partial_\tau^{1/2}$ designates the fractional time derivative operator of half-order given by

$$\partial_\tau^{1/2} f(\tau) = \frac{1}{\sqrt{\pi}}\partial_\tau \int_0^\tau \frac{f(s)}{\sqrt{\tau - s}}\,\mathrm{d}s = \frac{1}{\sqrt{\pi}}\int_0^\tau \frac{f'(s)}{\sqrt{\tau - s}}\,\mathrm{d}s$$

if $f(0) = 0$. See [11] for details.

Now utilizing (10) as a boundary condition and imposing it on the boundary point b, and repeating the above deduction for the boundary point a, we can derive a new problem, which is only defined in the finite computational interval $\Omega = (a,b)$

$$\begin{aligned} &\mathrm{i}\partial_t q + \partial_x^2 q - 2\rho|q|^2 q = 0 \quad \text{in } \Omega,\ t > 0, \\ &\partial_n q(x,t) = \mathscr{K}(t; q(x,\cdot)) \ \text{ on } \Sigma,\ t > 0, \\ &q(x,0) = q_0(x) \ \text{ in } \Omega. \end{aligned} \tag{13}$$

According to our analysis, its solution is exactly the same as that of the original problem (1) restricted to Ω.

3. Numerical issues

When one tries to numerically solve the problem (13), three issues have to be considered:

1. the discretization method for the cubic NLS equation;
2. the approximation method for the DtN operator $\mathscr{K}$ in the discrete level;
3. the match of the two selections made above.

The first two issues typically concern with accuracy and efficiency of different numerical choices, while the last one is much related to the stability of the overall scheme, since for the linear Schrödinger equation, an improper match of the discretization of NRBCs and the interior discretization will lead to a loss of stability, even if the unconditionally stable Crank–Nicolson scheme is used to discretize the equation (see [15]). In the following, we discuss these issues in detail.

3.1. Discretization of the cubic NLS equation

Many articles have been devoted to the numerical study of the Schrödinger-type equations utilizing different time discretizations. Two popular cases use schemes of time-splitting type and Crank–Nicolson type. The most remarkable advantage of time-splitting-type schemes lies in the application of the FFT, a most valuable and notable numerical algorithm in the science and engineering. But this method requires some periodic boundary conditions to bound the computational domain, and it is surely not this case for our considered problem setting. The Crank–Nicolson-type schemes are of second order in time, and usually unconditionally stable in the sense of L^2-norm. Besides, for the whole space problems, they conserve the charge and the energy in the discrete level, which are two conserved quantities in the continuous version.

Based on the method of Strauss and Vázquez [18], Delfour et al. [8] proposed the first standard Crank–Nicolson scheme (referred to as CN-Delfour in the following) for the NLS equation, which reads

$$\mathrm{i}\frac{q^{n+1}-q^n}{\Delta t}+\partial_x^2\frac{q^{n+1}+q^n}{2}-2\rho\frac{|q^{n+1}|^2+|q^n|^2}{2}\frac{q^{n+1}+q^n}{2}=0, \tag{14}$$

where Δt denotes the time step and $q^n(x)$ denotes the approximation of $q(x,t_n)$ with $t_n=n\Delta t$. Based on the discretization of q by the mid-point rule, Durán and Sanz-Serna [9] proposed another Crank–Nicolson-type scheme (CN–Durán–Sanz-Serna)

$$\mathrm{i}\frac{q^{n+1}-q^n}{\Delta t}+\partial_x^2\frac{q^{n+1}+q^n}{2}-2\rho\left|\frac{q^{n+1}+q^n}{2}\right|^2\frac{q^{n+1}+q^n}{2}=0, \tag{15}$$

which is well adapted for computing soliton-like solutions. Notice that these two schemes are globally nonlinearly implicit, and at each time step, an iterative procedure is needed to be performed. Comparatively, Zhang et al. [20] proposed a three-stage Leap–Frog time discretization

$$\mathrm{i}\frac{q^{n+1}-q^{n-1}}{2\Delta t}+\partial_x^2\frac{q^{n+1}+q^{n-1}}{2}-2\rho|q^n|^2\frac{q^{n+1}+q^{n-1}}{2}=0. \tag{16}$$

This scheme is still of second order and good conservation properties, but only globally linearly implicit, thus then a direct solver based on the LU decomposition can be employed in the computation. A drawback of this scheme is that it is not selfstarting, in the sense that q^1 has to be provided by some other scheme such as Cauchy iteration or the Crank–Nicolson linearly implicit scheme with a small time step. To avoid this special treatment, Besse [7] designed a relaxation scheme (CN-Besse)

$$\mathrm{i}\frac{q^{n+1}-q^n}{\Delta t}+\partial_x^2\frac{q^{n+1}+q^n}{2}-2\rho\phi^{n+\frac{1}{2}}\frac{q^{n+1}+q^n}{2}=0, \tag{17}$$

with $\phi^{n+\frac{1}{2}}$ given by

$$\phi^{\frac{1}{2}} = |q^0|^2, \quad \phi^{n+\frac{1}{2}} = 2|q^n|^2 - \phi^{n-\frac{1}{2}}.$$

3.2. Approximation of the DtN operator $\mathscr{K}$

We first address on how to evaluate the unknown functions $\{L_j(t,s)\}_{j=1,2}$ and $\{M_j(t,s)\}_{j=1,2}$ in Eqs. (4)–(9), provided that $g_0(t)$ and $g_1(t)$ are prescribed. For any function $A(\cdot,\cdot)$ defined in

$$\{(t,s) : -t \leqslant s \leqslant t, 0 \leqslant t \leqslant N\Delta t = T_f\},$$

we let $A_j^n \sim A(t_n, -t_n + 2j\Delta t)$, $j = 0,1,\ldots,n$. Here, T_f denotes the ending time point. Besides, we let $g_0^n \sim g_0(t_n)$ and $g_1^n \sim g_1(t_n)$. Note that $\frac{1}{\sqrt{2}}(A_t + A_s) = (\frac{1}{\sqrt{2}}, \frac{1}{\sqrt{2}}) \cdot \nabla A$ is the directional derivative of A with angle $\frac{\pi}{4}$, and $\frac{1}{\sqrt{2}}(A_t - A_s) = (\frac{1}{\sqrt{2}}, -\frac{1}{\sqrt{2}}) \cdot \nabla A$ is that with angle $-\frac{\pi}{4}$. From Eq. (7) and the boundary conditions (4), we have $M_1(t,-t) = M_1(0,0) = 0$. Then from Eq. (5), we have $L_1(t,-t) = L_1(0,0) = 0$. Thus naturally, we set

$$L_{1,0}^n = M_{1,0}^n = 0. \tag{18}$$

From Eq. (8), $M_2(t,t)$ can be integrated out explicitly since $L_1(t,t)$ and $M_1(t,t)$ are known functions. Then, from Eq. (6), $L_2(t,t)$ can be computed. To evaluate them numerically, we use the trapezoidal scheme, i.e. we solve $M_{2,n}^n$ from

$$\frac{M_{2,n}^n - M_{2,n-1}^{n-1}}{\Delta t} = \rho\bar{g}_{0c}(L_{1,n}^n + L_{1,n-1}^{n-1}) - \mathrm{i}\rho\bar{g}_{1c}\frac{M_{1,n}^n + M_{1,n-1}^{n-1}}{2} \tag{19}$$

with

$$g_{0c} = \frac{g_0^n + g_0^{n-1}}{2}, \quad g_{1c} = \frac{g_1^n + g_1^{n-1}}{2},$$

and then, we solve $L_{2,n}^n$ from

$$\frac{L_{2,n}^n - L_{2,n-1}^{n-1}}{\Delta t} = -\mathrm{i}\rho\bar{g}_{1c}\frac{L_{1,n}^n + L_{1,n-1}^{n-1}}{2} - \alpha_c\frac{M_{2,n}^n + M_{2,n-1}^{n-1}}{2} + \rho\bar{\beta}_c\frac{M_{1,n}^n + M_{1,n-1}^{n-1}}{2} \tag{20}$$

with

$$\alpha_c = \frac{\rho}{2}(g_{0c}\bar{g}_{1c} - \bar{g}_{0c}g_{1c}), \quad \beta_c = \frac{\mathrm{i}}{2}\left(\frac{g_0^n - g_0^{n-1}}{\Delta t} + \mathrm{i}\rho|g_{0c}|^2 g_{0c}\right).$$

To compute $\{L_{1,j}^n, M_{1,j}^n, L_{2,j}^n, M_{2,j}^n\}_1^{n-1}$, we could employ the same trapezoidal scheme for PDEs (5)–(8) to get a second order approximation:

$$\frac{L_{1,j}^n - L_{1,j}^{n-1}}{\Delta t} = \mathrm{i}g_{1c}\frac{L_{2,j}^n + L_{2,j}^{n-1}}{2} + \alpha_c\frac{M_{1,j}^n + M_{1,j}^{n-1}}{2} + \beta_c\frac{M_{2,j}^n + M_{2,j}^{n-1}}{2}, \tag{21}$$

$$\frac{L_{2,j}^n - L_{2,j-1}^{n-1}}{\Delta t} = -\mathrm{i}\rho\bar{g}_{1c}\frac{L_{1,j}^n + L_{1,j-1}^{n-1}}{2} - \alpha_c\frac{M_{2,j}^n + M_{2,j-1}^{n-1}}{2} + \rho\bar{\beta}_c\frac{M_{1,j}^n + M_{1,j-1}^{n-1}}{2}, \tag{22}$$

$$\frac{M_{1,j}^n - M_{1,j}^{n-1}}{\Delta t} = 2g_{0c}\frac{L_{2,j}^n + L_{2,j}^{n-1}}{2} + \mathrm{i}g_{1c}\frac{M_{2,j}^n + M_{2,j}^{n-1}}{2}, \tag{23}$$

$$\frac{M_{2,j}^n - M_{2,j-1}^{n-1}}{\Delta t} = 2\rho\bar{g}_{0c}\frac{L_{1,j}^n + L_{1,j-1}^{n-1}}{2} - \mathrm{i}\ \rho\bar{g}_{1c}\frac{M_{1,j}^n + M_{1,j-1}^{n-1}}{2}. \tag{24}$$

But this choice will necessitate solving a $4(n-1)$-order system of linear algebraic equations on the nth time step, which is too expensive if the number of the time steps is large, since any direct solver based on Gauss elimination requires $O(n^3)$ operations. Instead of the trapezoidal scheme, we can employ its explicit counterpart with the predictor–corrector technique. That is to say, we first use the Euler scheme to derive the first-order approximations $\{L_{1,j,*}^n, M_{1,j,*}^n, L_{2,j,*}^n, M_{2,j,*}^n\}_1^{n-1}$

$$\frac{L^n_{1,j,*} - L^{n-1}_{1,j}}{\Delta t} = \mathrm{i}g_{1c}L^{n-1}_{2,j} + \alpha_c M^{n-1}_{1,j} + \beta_c M^{n-1}_{2,j}, \tag{25}$$

$$\frac{L^n_{2,j,*} - L^{n-1}_{2,j-1}}{\Delta t} = -\mathrm{i}\rho\bar{g}_{1c}L^{n-1}_{1,j-1} - \alpha_c M^{n-1}_{2,j-1} + \rho\bar{\beta}_c M^{n-1}_{1,j-1}, \tag{26}$$

$$\frac{M^n_{1,j,*} - M^{n-1}_{1,j}}{\Delta t} = 2g_{0c}L^{n-1}_{2,j} + \mathrm{i}g_{1c}M^{n-1}_{2,j}, \tag{27}$$

$$\frac{M^n_{2,j,*} - M^{n-1}_{2,j-1}}{\Delta t} = 2\rho\bar{g}_{0c}L^{n-1}_{1,j-1} - \mathrm{i}\rho\bar{g}_{1c}M^{n-1}_{1,j-1}, \tag{28}$$

then we compute $\{L^n_{1,j}, M^n_{1,j}, L^n_{2,j}, M^n_{2,j}\}_1^{n-1}$ by replacing those of them appearing in the right hand side of Eqs. (21)–(24) with $\{L^n_{1,j,*}, M^n_{1,j,*}, L^n_{2,j,*}, M^n_{2,j,*}\}_1^{n-1}$

$$\frac{L^n_{1,j} - L^{n-1}_{1,j}}{\Delta t} = \mathrm{i}g_{1c}\frac{L^n_{2,j,*} + L^{n-1}_{2,j}}{2} + \alpha_c\frac{M^n_{1,j,*} + M^{n-1}_{1,j}}{2} + \beta_c\frac{M^n_{2,j,*} + M^{n-1}_{2,j}}{2}, \tag{29}$$

$$\frac{L^n_{2,j} - L^{n-1}_{2,j-1}}{\Delta t} = -\mathrm{i}\rho\bar{g}_{1c}\frac{L^n_{1,j,*} + L^{n-1}_{1,j-1}}{2} - \alpha_c\frac{M^n_{2,j,*} + M^{n-1}_{2,j-1}}{2} + \rho\bar{\beta}_c\frac{M^n_{1,j,*} + M^{n-1}_{1,j-1}}{2}, \tag{30}$$

$$\frac{M^n_{1,j} - M^{n-1}_{1,j}}{\Delta t} = 2g_{0c}\frac{L^n_{2,j,*} + L^{n-1}_{2,j}}{2} + \mathrm{i}g_{1c}\frac{M^n_{2,j,*} + M^{n-1}_{2,j}}{2}, \tag{31}$$

$$\frac{M^n_{2,j} - M^{n-1}_{2,j-1}}{\Delta t} = 2\rho\bar{g}_{0c}\frac{L^n_{1,j,*} + L^{n-1}_{1,j-1}}{2} - \mathrm{i}\rho\bar{g}_{1c}\frac{M^n_{1,j,*} + M^{n-1}_{1,j-1}}{2}. \tag{32}$$

Comparatively, this scheme only requires O(n) operations, but is still of second order.

Next, we consider the approximation of the integral in Eq. (12). The difficulty lies in the treatment of the half-order derivative, which is strongly related to the DtN mapping of the linear free Schrödinger equation. In [6], based on the piecewise linear interpolation of the unknown function, Baskakov and Popov proposed a discretization method of 1.5th order for its half-order derivative. More recently, Antoine and Besse [3] gave another kind of approximation of the half-order derivative based on the semi-discretization of the free Schrödinger equation in time. Compared with the former, the latter not only has a higher accuracy of second order, but leads to an unconditionally stable numerical scheme when cooperating with the interior Crank–Nicolson discretization for the free Schrödinger equation, while the former generally leads to a loss of stability (see [15]). Utilizing either of these two methods, we derive the following approximation of Eq. (12)

$$g^n_1 = g^n_0 M^n_{2,n} - \mathrm{e}^{-\mathrm{i}\pi/4}\frac{2}{\sqrt{2\Delta t}}\sum_{j=0}^{n}\alpha_j M^n_{1,n-j} \tag{33}$$

where

$$\alpha_j = \begin{cases} \sqrt{\frac{2}{\pi}} & j = 0, \\ \sqrt{\frac{2}{\pi}}\left(\frac{1}{\sqrt{j+1}+\sqrt{j}} - \frac{1}{\sqrt{j}+\sqrt{j-1}}\right) & j > 0. \end{cases}$$

for the Baskakov–Popov method [6] and

$$\alpha_j = \begin{cases} \frac{(2k)!}{2^{2k}(k!)^2}, & j = 2k, \\ -\alpha_{j-1}, & j = 2k+1. \end{cases}$$

for the Antoine–Besse method [3].

Now we come to the approximation of the DtN operator $\mathscr{K}$ involved in (10). $\mathscr{K}$ is essentially a nonlinear operator, and it must be evaluated by some iterative technique. Although other possibilities could be explored, we present here a successive approximation method. Though simple, it turns out to be very efficient by our numerical tests. For reference, we denote this approximation by $\mathscr{K}_{\Delta t}$ in the following:

Box 1. Successive approximation method for computing $g_1^n = \mathcal{K}_t(t_n, \{g_0^j\}_0^n)$.

if $n = 0$, then
  Set $g_1^n = 0$, $L_{1,0}^0 = M_{1,0}^0 = L_{2,0}^0 = M_{2,0}^0 = 0$
else
  Let $g_1^n = g_1^{n-1} = \mathscr{K}_{\Delta t}(t_{n-1}, \{g_0^j\}_0^{n-1})$ initially
  do
    compute $\{L_{1,j}^n, M_{1,j}^n, L_{2,j}^n, M_{2,j}^n\}_0^n$ from (4), (18), (19), (20), (26)–(32)
    set $v = g_0^n M_{2,n}^n - e^{-i\pi/4}\frac{2}{\sqrt{2\Delta t}}\sum_{j=0}^n \alpha_j M_{1,n-j}^n$
    if $|v - g_1^n| < \epsilon$, exit
    else, set $g_1^n = v$
    end if
  end do

3.3. Match of the interior discretization and the approximation of the DtN mapping

Formally, we can couple any of the interior Crank–Nicolson-type discretizations with the discretized DtN operator $\mathscr{K}_{\Delta t}$ to derive an overall scheme for the problem (13). Any choice will leads to a system of essentially nonlinear equations. Since the according Jacobian is complicated to obtain, we propose a successive approximation method, which is adapted from the algorithm in Table 4.1 of [3].

Box 2. Algorithm for solving the cubic NLS with the exact NRBCs.

let $q^{n+1} = q^n$ initially
do
  solve the linear boundary-value problem

$$\begin{cases} i\frac{w-q^n}{\Delta t} + \partial_x^2\frac{w+q^n}{2} = \Phi_{n+\frac{1}{2}}(q^n, q^{n+1})\frac{q^{n+1}+q^n}{2} & \text{in } \Omega, \\ \partial_n w + e^{-i\pi/4}\frac{2}{\sqrt{2\Delta t}} w = \mathscr{K}_{\Delta t}(t_{n+1}, \{q^j\}_0^{n+1}) + e^{-i\pi/4}\frac{2}{\sqrt{2\Delta t}} q^{n+1} & \text{on } \Sigma, \end{cases} \tag{34}$$

  if $\|w - q^{n+1}\|_{L^2(\Omega)} < \epsilon$, set $q^{n+1} = w$, and exit
  else, set $q^{n+1} = w$
  end if
end do

The function $\Phi_{n+\frac{1}{2}}$ in Box 2 is defined as

$$\Phi_{n+\frac{1}{2}}(q^n, q^{n+1}) = \begin{cases} \rho(|q^n|^2 + |q^{n+1}|^2) & \text{for CN–Delfour,} \\ \rho\frac{|q^n+q^{n+1}|^2}{2} & \text{for CN–Durán–Sanz-Serna,} \\ 4\rho|q^n|^2 - \Phi_{n-\frac{1}{2}}(q^{n-1}, q^n) & \text{for CN–Besse with } \Phi_{\frac{1}{2}} = 2\rho|q^0|^2. \end{cases} \tag{35}$$

We write the NRBCs as Robin-type intentionally, since our vast numerical tests show that when cooperating this kind of boundary conditions, the system (34) has a good local convergence property.

The system (34) can be solved either by finite difference method (FD) or by finite element method (FEM). Thus, for different choices of the interior time and space discretization and for different choices of the discretized DtN operator, we get a series of different numerical schemes. For convenience of reference, we combine

these choices together to denote the specific scheme. For example, if scheme CN-Durán–Sanz-Serna is used for time discretization and the conform linear finite element is used for spatial discretization, the scheme is abbreviated to Durán–Sanz-Serna-FEM1. And if method Antoine–Besse is further specified for the approximation of the DtN operator $\mathscr{K}$, the scheme is denoted by Durán–Sanz-Serna-FEM1–Antoine–Besse.

As revealed by Mayfield, an improper match of the interior discretization and the approximation of the NRBCs would generally lead to a loss of stability for the linear Schrödinger equation, even if the interior discretization is unconditionally stable for the whole space problem. This might also happen for our proposed scheme. But in our numerical tests, we do not observe this phenomenon. A further study is still under investigation.

4. Numerical experiments

The one-dimensional cubic nonlinear Schrödinger equation is integrable, and theoretically, it can be solved with the inverse scattering theory. For the focusing case, this approach yields the exact soliton solution given by

$$q_{\text{exa}}(x,t) = \sqrt{a}\,\text{sech}(\sqrt{a}(x-ct))\mathrm{e}^{\frac{ic}{2}x+(a-\frac{c^2}{4})t}. \tag{36}$$

The real parameter a is the amplitude of the wavefield, and c is the velocity of the soliton. We will take it as a reference solution to test the accuracy of our numerical scheme, since this solution decays exponentially fast with respect to the spatial variable, and it can be taken as a "compact" function at the initial time, as required by our problem setting.

In all the numerical tests, we take $\epsilon = 10^{-6}$ for both algorithms in Box 1 and Box 2. The computation is performed on a personal computer with a 1.70 GHz CPU and 1GB of memory.

4.1. Tests on the discrete DtN operator $\mathscr{K}_{\Delta t}$

First, we consider the computational aspects of the nonlinear DtN mapping. Let $a = 2$ and $c = 15$ in the soliton expression (36). In $(X, +\infty)\times(0,1)$ with $X = 10$, $q_{\text{exa}}(x,0)$ is equal to zero function with a tolerance of 2.043×10^{-6}. Thus, if letting $g_0(t) = q_{\text{exa}}(X,t)$, the exact Neumann function $g_{1,\text{exa}}(t)$ can be taken to be $\partial_x q_{\text{exa}}(X,t)$. Now we use the algorithm in Box 1 to compute the numerical approximation of $g_{1,\text{exa}}(t)$ on the time interval [0,2].

Table 1 lists the numerical statistics for different time steps when either of the two approximation methods is employed. Row "Error" lists the relative errors at the time point $t = 0.8$. From this table, we see that method Antoine–Besse has a higher accuracy than method Baskakov–Popov, just as anticipated above. Since the number of iterations, denoted by i_n at the nth time step, are different at different time steps, and the number of operations for each iteration is $O(n)$, for comparison, we define the average number of iterations (Ite. Num.) as $\frac{\sum_{n=1}^{N} n i_n}{\sum_{n=1}^{N} n}$. Row "Time" lists the total computation time given in unit of second. From Table 1, we see that the successive approximation algorithm of the discretized DtN operator is quite satisfactory. The average number

Table 1
Numerical statistics on the discretized DtN operator

Time step Δt	0.01	0.005	0.0025	0.00125
Baskakov–Popov				
Error	4.624E−2	2.270E−2	9.537E−3	3.730E−3
Order	–	1.027	1.251	1.355
Ite. num.	3.066	2.654	2.284	2.081
Time	0.02	0.06	0.22	0.87
Antoine–Besse				
Error	1.797E−2	4.523E−3	1.134E−3	2.850E−4
Order	–	1.991	1.996	1.993
Ite. num.	3.478	3.075	2.865	2.680
Time	0.02	0.08	0.27	1.09

of iterations is generally less than 4. We should remark here that this is also almost true for other numerical tests.

In Fig. 1, the absolute error functions are plotted for these two methods. The time step is set to be $\Delta t = 0.005$. We see that method Antoine–Besse is much more accurate than method Baskakov–Popov. Besides, instability is not detected in this numerical test.

4.2. Tests on the successive approximation algorithm in Box 2

We let $\Omega = (-10,10)$, $a = 2$, $c = 15$, $T_f = 2$ and $q_0(x) = q_{\text{exa}}(x,0)$. Owing to the same reason as in 4.1, the exact solution can be taken as $q_{\text{exa}}(x,t)$.

To explore the convergence rate in space, we let the time step be extremely small, $\Delta t = 0.0001$. Fig. 2 shows the absolute L^2 errors at $t = 0.7$. At this time point, more than 80 percent of the total charge has moved out the computational domain. From this figure, we observe a second-order decrease of the errors for any of the employed schemes, no matter which approximation is used for the discretized DtN operator. To explore the

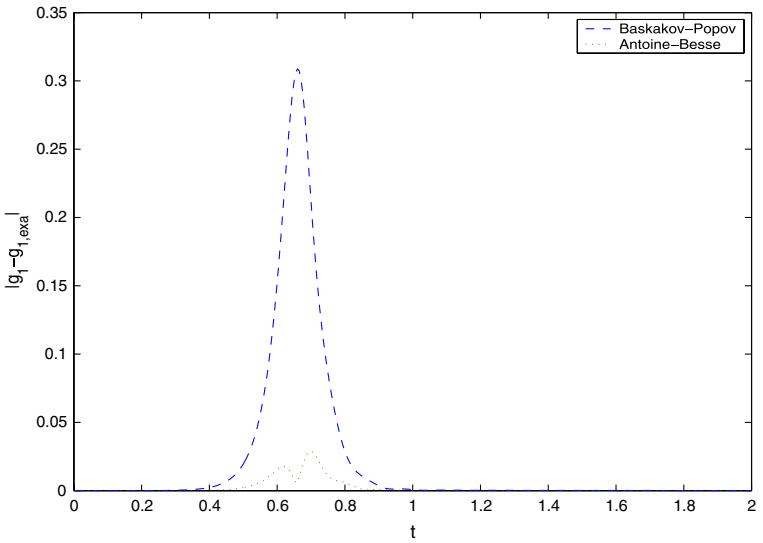

Fig. 1. Absolute errors.

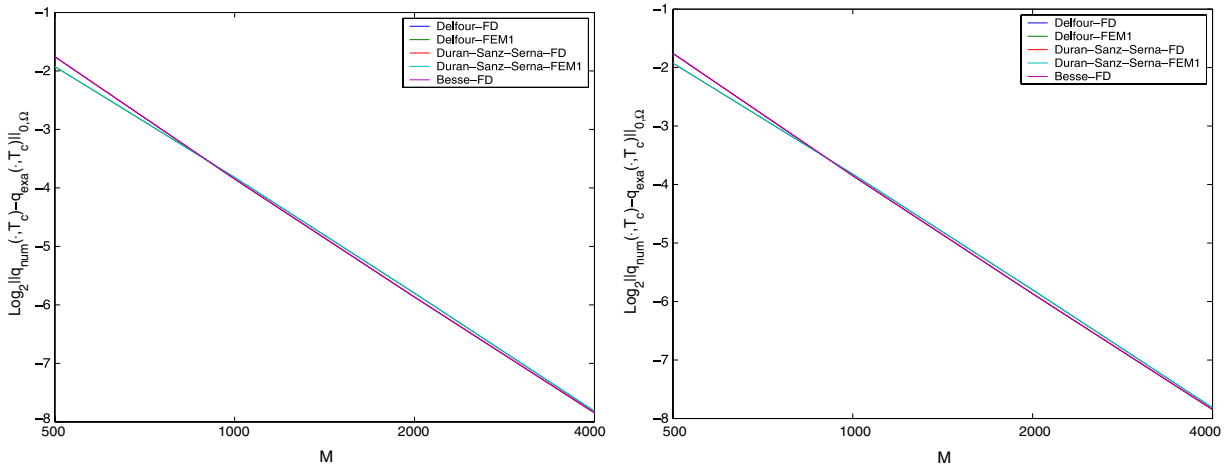

Fig. 2. Absolute errors of spatial discretizations. Left: Baskakov–Popov method. Right: Antoine–Besse method.

convergence rate in time, the number of the grid points is set to be $M = 400000$. Fig. 3 shows the numerical results. A second-order accuracy in time can be observed for any of the proposed schemes.

Next, we study the error change process with the time evolution. Let $\Delta t = 0.001$, $M = 4000$. Fig. 4 shows the evolution of the absolute errors. We see that before the time point $t = 0.5$, when the soliton is still a little far away from the boundary points, the boundary conditions do not take into effect, and the errors are accumulated almost linearly. We would remark that this process is typical when numerically solving any of the time-dependent problems, and it is not originated from any kind of the possibly-existing instability properties of the numerical schemes. After time $t = 0.5$, owing to the wonderfully nonreflecting property of the artificial boundary conditions, the charge moves out the computational domain, and accordingly, the errors drops after time $t = 0.6$. In the end, after time $t = 1.0$ when most of the charge moves out, the errors nearly remain a constant value. For method Baskakov–Popov used to discretize the DtN operator, this value is almost 0.002, while for method Antoine–Besse, this value is less than 1.1×10^{-4}. Thus, compared with method Baskakov–Popov, method Antoine–Besse presents numerical solutions with less reflections. We plot the amplitude of the soliton in Fig. 5 with scheme Durán–Sanz-Serna-FEM1–Antoine–Besse. No observable reflections can be detected at all.

Table 2 lists some numerical statistics, where M. num. stands for the maximal iteration number in the algorithm in Box 2, while A. num. stands for the average iteration number. We see that compared with method

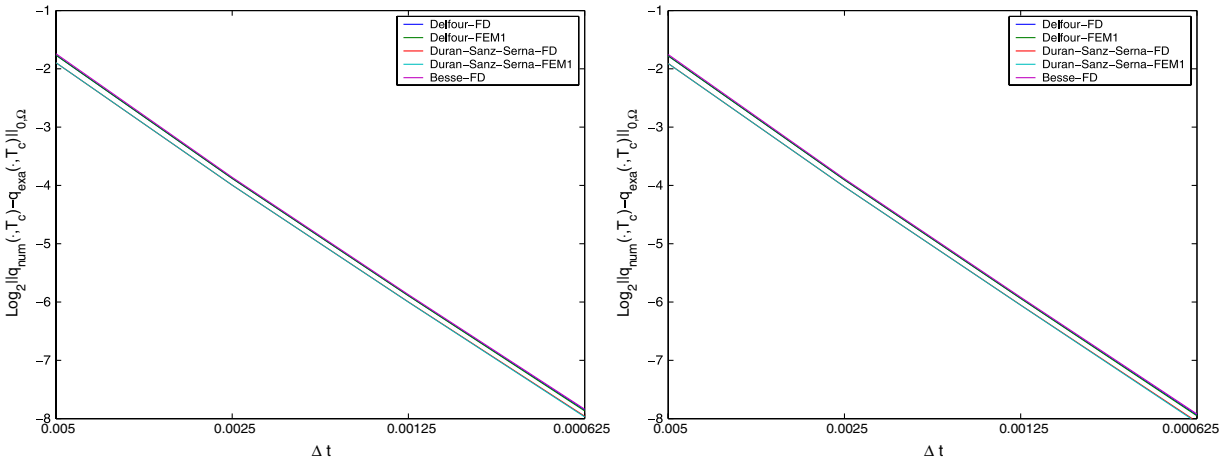

Fig. 3. Absolute errors of time discretizations. Left: Baskakov–Popov method. Right: Antoine–Besse method.

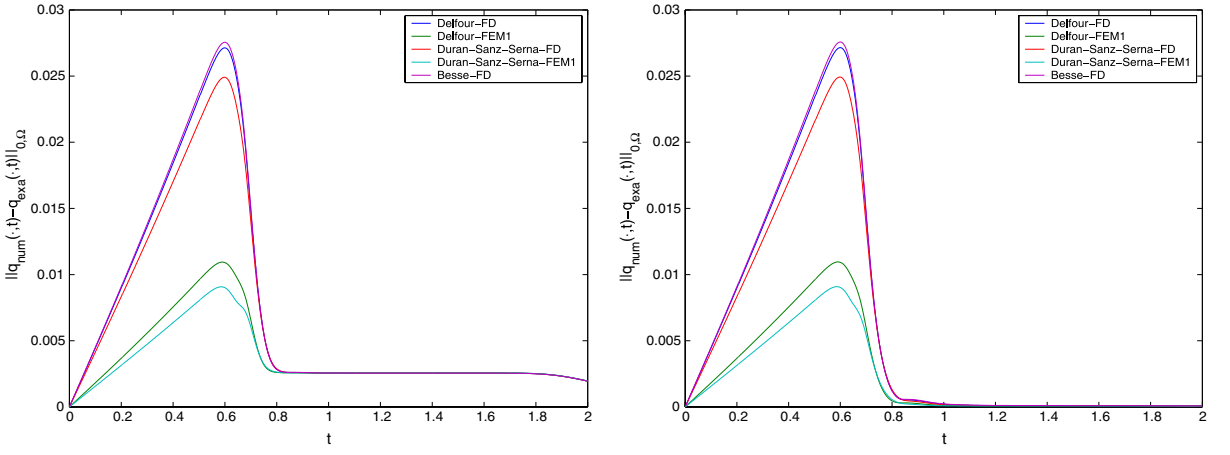

Fig. 4. Evolution of the absolute errors for a "fast" soliton.

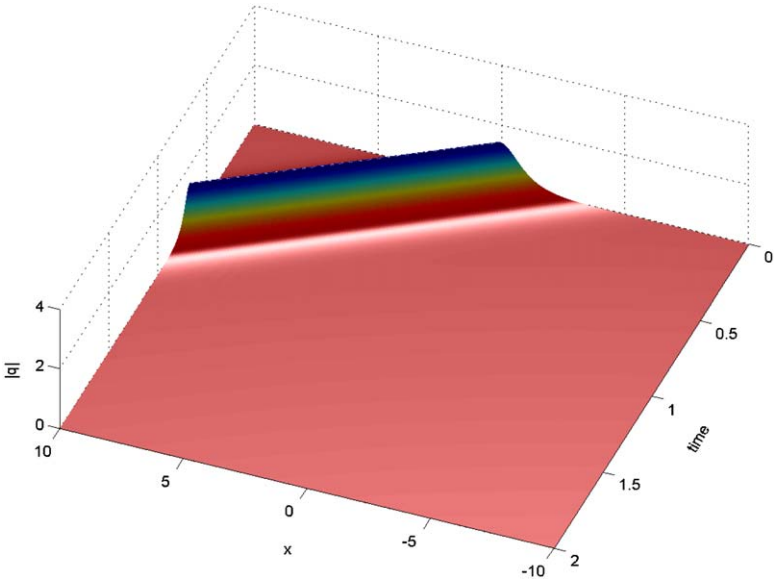

Fig. 5. Evolution of the amplitude of a "fast" soliton.

Table 2
Numerical statistics

	Baskakov–Popov			Antoine–Besse		
	M. num.	A. num.	Time	M. num.	A. num.	Time
Delfour-FD	6	2.939	16	3	2.385	14
Delfour-FEM1	6	2.939	21	3	2.385	18
Durán–Sanz-Serna-FD	6	2.939	16	3	2.385	14
Durán–Sanz-Serna-FEM1	6	2.939	21	3	2.385	19
Besse-FD	6	2.932	16	3	2.382	15

$\Delta t = 0.001$, $M = 4000$ and $T_f = 2$.

Baskakov–Popov, method Antoine–Besse typically leads to less iterations, which is another remarkable advantage of this approximation.

For comparison, we also plot in Fig. 6 the errors of the numerical solution of a "slow" soliton with a speed $c = 4$. The time step is 0.001 and the number of grid points is $M = 4000$, same as those used for the "fast"

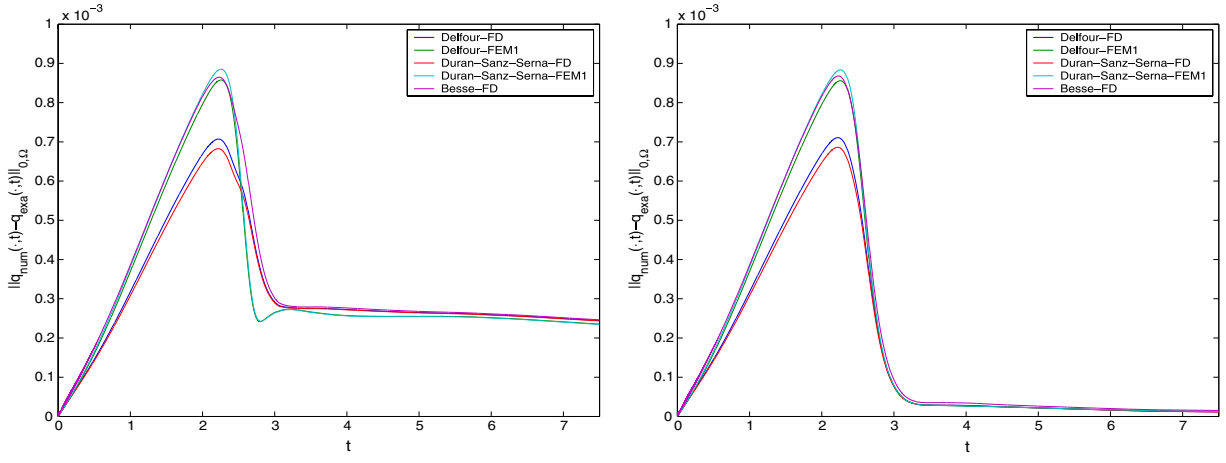

Fig. 6. Evolution of the absolute errors for a "slow" soliton.

soliton. The ending time point is $T_f = 7.5$. Again, we observe that method Antoine–Besse leads to less reflections compared with method Baskakov–Popov, even the latter has already presented a fairly good approximation. Besides, comparing Fig. 7 with Fig. 5, We observe that for the same computational parameters Δt and M, we get a higher resolution for a "slow" soliton. This is much different from the behaviour of the approximate NRBCs designed by Antoine, Besse and Descombes [3]. Since their NRBCs are designed under a high-frequency assumption, their approach is more efficient for a high speed soliton, and their numerical tests also verify this point. On the contrary, since our NRBCs are exactly nonreflecting in their continuous form, a "slow" soliton has a better resolution than a "fast" one in time when their time steps are the same value. Fig. 7 shows the results with scheme Durán–Sanz-Serna-FEM1–Antoine–Besse. Again, no reflections can be observed.

We would also remark that no instability is observed from our vast numerical tests.

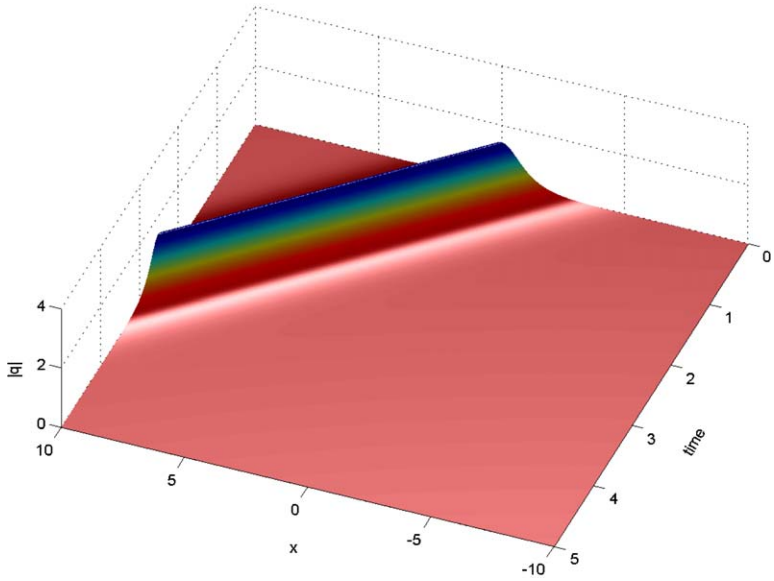

Fig. 7. Evolution of the amplitude of a "slow" soliton.

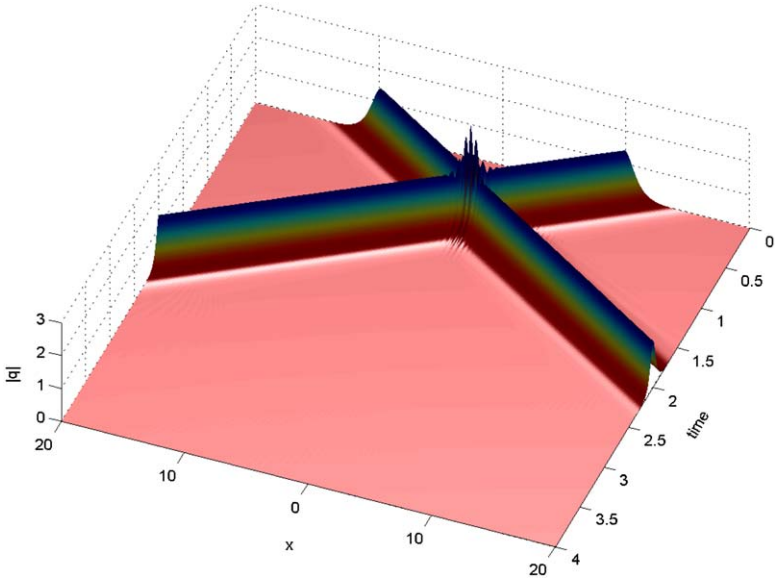

Fig. 8. Interaction of two "fast" solitons with opposite directions.

4.3. Application to the soliton interaction

Finally, we use scheme Durán–Sanz-Serna-FEM1–Antoine–Besse to simulate the interaction of two solitons. This problem has been investigated by Antoine, Besse and Descombes [3] to show the robustness of their approach. We repeat this experiment here to fulfill the same purpose. The computational interval is set to be $\Omega = [-20,20]$. $\Delta t = 0.001$ and $M = 8000$. The amplitudes of the solitons are of the same value $a = 2$, and in each test case, two solitons are initially located at $x = -10$ and $x = 10$, respectively. Fig. 8 shows the interaction of two "fast" solitons with the speed $|c| = 15$ which travel with opposite directions. Fig. 9 shows the interaction of a "fast" soliton and a "slow" soliton with opposite directions. Their velocities are $c = 15$ and $c = -4$. Fig. 10 shows the interaction of a "fast" soliton and a "slow" soliton with same directions. Their velocities are

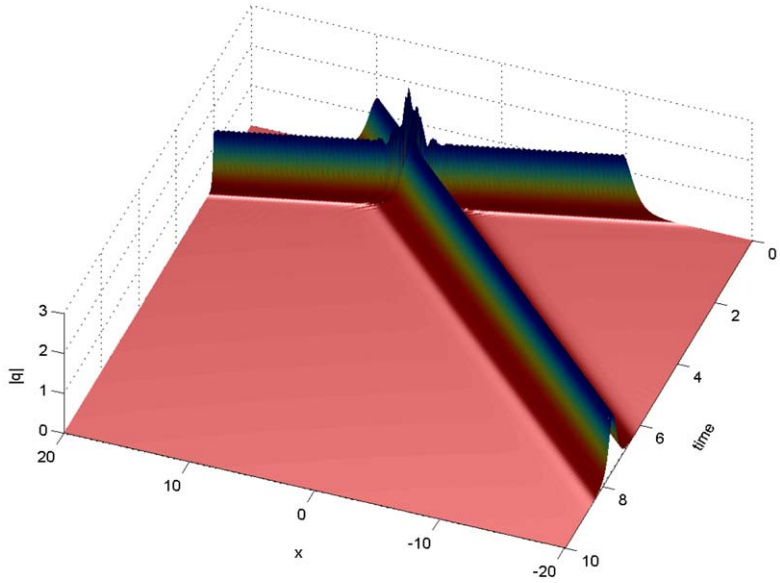

Fig. 9. Interaction of a "fast" soliton and a "slow" soliton with opposite directions.

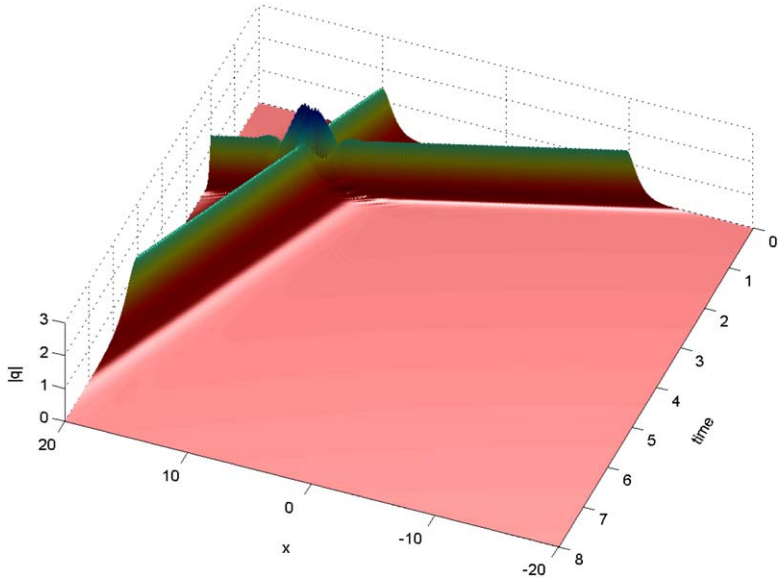

Fig. 10. Interaction of a "fast" soliton and a "slow" soliton with same directions.

$c = 15$ and $c = 2$. From these figures, we can not find any observable reflections on the boundary points, even an artifical light is added to each figure to show its refined structure.

5. Conclusion

We have derived a kind of exact nonreflecting boundary conditions for one-dimensional cubic nonlinear Schrödinger equations. They are based on the work of Boutet de Monvel at el. on the nonlinear spectral analysis of NLS on the half-line. We have designed a series of numerical schemes, which are all second order both in time and in space, as verified by our numerical experiments. Besides, we have used our scheme to simulate the evolution of the solitons, and the results show the robustness of our approach.

In fact, the idea of Boutet de Monvel at el. is applicable for some other nonlinear evolution PDEs defined in unbounded domains. We are hopeful that our idea for the cubic NLS can be adapted to these problems. Besides, it seems more promising to extend our approach to higher-dimensional problems. All these are now under investigation, and the results will be reported in the near future.

Acknowledgements

The author would like to thank Professor Houde Han for fruitful discussions on the algorithm listed in Box 1, and thank Professor Anton Arnold for referring him to the paper [3], and also thank Professor Ruiliang Lin for discussions on the inverse scattering transformation. Besides, the author is profoundly grateful to the anonymous reviewers. Their expert comments and suggestions have greatly improved the quality of this paper. Supported partially by the National Natural Science Foundation of China under Grant No. 10401020.

References

[2] X. Antoine, C. Besse, Unconditionally stable discretization schemes of non-reflecting boundary conditions for the one-dimensional Schrödinger equation, J. Comput. Phys. 181 (1) (2003) 157–175.
[3] X. Antoine, C. Besse, S. Descombes, Artificial boundary conditions for one-dimensional cubic nonlinear Schrödinger equations, SIAM J. Numer. Anal. (in press).
[4] M. Erhardt, A. Arnold, Discrete transparent boundary conditions for the Schrödinger equation, Riv. Math. Univ. Parma 6 (4) (2001) 57–108.
[5] W. Bao, S. Jin, P.A. Markowich, On time-splitting spectral approximations for the Schrödinger equation in the semiclassical regime, J. Comput. Phys. 175 (2002) 487–524.
[6] V.A. Baskakov, A.V. Popov, Implementation of transparent boundaries for the numerical solution of the Schrödinger equation, Wave Motion 14 (1991) 123–128.
[7] C. Besse, A relaxation scheme for the nonlinear Schrödinger equation, SIAM J. Numer. Anal. 42 (3) (2004) 934–952.
[8] M. Delfour, M. Fortin, G. Payre, Finite-difference solutions of a nonlinear Schrödinger equation, J. Comput. Phys. 44 (1981) 277–288.
[9] A. Durán, J.M. Sanz-Serna, The numerical integration of relative equilibrium solution. The nonlinear Schrödinger equation, IMA J. Numer. Anal. 20 (2) (2000) 235–261.
[10] A. Boutet de Monvel, A.S. Fokas, D. Shepelsky, Analysis of the global relation for the nonlinear Schrödinger equation on the half-line, Lett. Math. Phys. 65 (2003) 199–212.
[11] R. Gorenflo, F. Mainardi, Fractional calculus: integral and differential equations of fractional order, in: A. Carpinteri, F. Mainardi (Eds.), Fractals and Fractional Calculus in Continuum Mechanics, Springer, Wien, 1997.
[12] H.D. Han, Z.Y. Huang, Exact artificial boundary conditions for Schrödinger equation in $\mathbf{R}^2$, Commun. Math. Sci. 2 (1) (2004) 79–94.
[13] H. Hasimoto, A soliton on a vortex filament, J. Fluid. Mech. 51 (1972) 477–485.
[15] B. Mayfield, Non local boundary conditions for the Schrödinger equation, PhD thesis, University of Rhodes Island, Providence, RI, 1989.
[16] C. Peskin, D. McQueen, Mechanical equilibrium determines the fractal fiber architecture of aortic heart leaflets, Am. J. Physiol. 266 (1994) 319–328.
[18] W.A. Strauss, L. Vázquez, Numerical solution of a nonlinear Klein–Gordon equation, J. Comput. Phys. 28 (1978) 271–278.
[19] J.A.C. Weideman, B.M. Herbst, Split-step methods for the solution of the nonlinear Schrödinger equation, SIAM J. Numer. Anal. 23 (1986) 485–507.
[20] F. Zhang, V.M. Pérez-García, L. Vázquez, Numerical simulation of nonlinear Schrödinger systems: a new conservative scheme, Appl. Math. Comput. 71 (1995) 165–177.